Journal of Heat and Mass Transfer Research 2 (2015) 59-70

Semnan University

Journal of Heat and Mass Transfer Research

Journal homepage: http://jhmtr.journals.semnan.ac.ir

Effects of the rectangular groove dimensions on the thermal features of the turbulent Al_2O_3-water nanofluid flow in the grooved tubes

Komayl Mohebbi , Roohollah Rafee*, Farhad Talebi

Faculty of Mechanical Engineering, Semnan University, Semnan

PAPER INFO

History:
Received 21 June 2015
Received in revised form 03 September 2015
Accepted 03 October 2015

Keywords:
Nanofluid
Grooved tube
Turbulent flow
Forced convection
Entropy generation minimization

A B S T R A C T

The forced convection heat transfer of turbulent Al_2O_3-water nanofluid flow inside the grooved tubes with the different aspect ratio of the rectangular grooves is numerically investigated. The governing equations have been solved using finite volume method (FVM) coupled with SIMPLE algorithm. It is assumed the heat flux is constant on the grooved walls. The Single-phase approach is applied for the computation of the nanofluid flow. The Nanoparticles volume fraction is in the range of 0-5% and flow Reynolds number is in the range of 10,000-35,000. Comparisons between the numerical results and available experimental data show that among different turbulence models, k-ε model with enhanced wall treatment gives the better results. The results show that the heat transfer coefficient increases with nanoparticles volume fraction and Reynolds number but it is accompanied by pressure drop augmentation. From the results, it is concluded that the grooved tubes with Al_2O_3-water nanofluid flow are thermodynamically advantageous. The Correlations for heat transfer coefficients have been presented for grooved tubes in different aspect ratios using the numerical results. The optimum geometric ratios in which the entropy generation is minimized are also determined.

1. Introduction

Nanofluids are used in many fields such as heat exchangers, automotive industry, aerospace, nuclear reactor, electronic cooling and refrigeration (See e.g. Cheng [1]). During past decade, many researchers investigated the methods to improve the heat transfer for engineering applications. The Different ways of the heat transfer enhancement are using the additives like nanoparticles and geometry modifications such as using grooves and wires in tubes or applying helical corrugated tubes. These modified geometries enhance the flow mixing due to chaotic movements and secondary flows from the wall to the core flow. Unfortunately, often by using these techniques, the pressure drop augmentation occurs as a penalty (See Duangthongsuk *et al.*[2]).

Enhancement of the heat transfer and pressure drop in the pipes with the rough surfaces was studied both experimentally and numerically in the literature. The Grooves are used in many devices like evaporators, heat exchangers, and solar air heaters (See e.g. Web *et al.* [3]). A review study of the heat transfer coefficient and pressure drop for different rib configurations was done by Dall Donne and Meyer [4]. Naphon *et al.* [5] experimentally studied the heat transfer and friction factor of the flow inside a heat exchanger with helical ribbed walls. They found that the effect of the corrugation height on the heat transfer and pressure drop is more than that of corrugation pitch. San and Huang [6] experimentally investigated the heat transfer enhancement of turbulent air flow inside the grooved tubes under isothermal surface condition. They presented the

Corresponding author: R. Rafee, Faculty of Mechanical Engineering, Semnan University, P.O.Box: 35131-19111, Semnan, Iran. Tel:, Fax: +982331533351
Email: *Rafee@semnan.ac.ir*

average Nusselt number and friction factor as a function of the ratio of the rib pitch to tube diameter (p/d) and rib height to tube diameter (e/d). Bilen *et al.* [7] made an experimental study on the heat transfer and friction characteristic of a fully developed turbulent air flow in a ribbed tube with different groove shapes (rectangular, trapezoidal and semi-circular). The Results showed that the use of the ribs enhances the heat transfer up to 63% for circular ribs, 58% for trapezoidal ribs and 47% for rectangular ribs, in comparison with the smooth tube. Also, they expressed that ribbed tubes are advantageous thermodynamically. Pingan *et al.*[8] used standard k-ε turbulent model with enhanced wall treatment to investigate the heat transfer of the air flow in channels with different rib shapes (semi-circular, rectangular and triangular) and observed that the average Nusselt number for the channels with triangular and rectangular ribs are the largest and smallest, respectively.

Choi [9] proposed the concept of nanofluids and the next researchers investigated the characteristics and properties of nanofluids extensively. Keblinski *et al.* [10] introduced four mechanisms that have contribution on the increase of the heat transfer of nanofluids: Brownian motion of the particles, molecular level layering at the liquid/particle interface, nature of nanofluid heat transfer, and clusters (high conductivity path). According to Das *et al.* [11], the heat transfer enhancement by nanofluids depends on several factors including the increment of thermal conductivity, nanoparticles type, size, shape, volume fraction, base fluid and flow regime. Pak and Cho [12], Xuan and Li [13] and Maiga *et al.* [14] presented correlations for the calculations of the nanofluid Nusselt number in tube as a function of Reynolds and Prandtl numbers in turbulent flows, which show the increase of convective heat transfer coefficient with the particles volume fraction and the flow Reynolds number.

Fotukian and Nasr Esfahany [15] showed that for the Al_2O_3-water nanofluid in turbulent flow under constant wall temperature conditions, the heat transfer and pressure drop are much greater than that of the base fluid. They reported 48% increment in the convective heat transfer rate. There are some studies focused on using both methods of heat transfer enhancement (using rough surface and nanofluids). For example, Wongcharee and Eisma-ard [16] experimentally studied the flow of CuO-water nanofluid inside corrugated tube under turbulent regime. They observed that for the mentioned geometry with 0.7% volume fraction of CuO, the heat transfer is 57% more than that of the plain tube. Manca *et al.* [17] carried out a numerical investigation on turbulent forced convection of the Al_2O_3-water nanofluid in ribbed channel with different rib shapes (square and rectangular). They showed that the heat transfer enhancement increases with the particle volume fraction and Reynolds number but it is accompanied by more pressure drop as a penalty. Vatani *et al.* [18] investigated the effects of various rib-groove shapes in a horizontal channel and the different types of nanofluids on thermal and hydraulic properties of flow numerically. Their results show that the rectangular rib-groove has the highest performance evaluation criterion (PEC) and the SiO_2-water nanofluid provides the highest Nusselt number among all studied types. In the study of Vatani and Mohammed [18], the PEC is defined as the ratio of Nusselt numbers in grooved and smooth channel over the ratio of skin friction coefficients in the grooved and smooth channels (i.e. $(Nu_g/Nu_s).(C_{fg}/C_{fs})^{-1}$). It means that a grooved channel with highest Nusselt number may have a large skin friction coefficient and may have lower PEC. Haghighi *et al.* [19] studied the heat transfer in the turbulent flow of the nanofluids inside tubes and claimed that at constant pumping powers, the nanofluid are not beneficial for cooling applications. Recently, Al-Shamani *et al.* [20] studied the convection heat transfer of the nanofluids in a channel with trapezoidal rib-grooves. They showed that their special trapezoidal groove (Trap +R-Trap G) has the highest Nusselt number in channel flow.

Nanofluids reduce the heat transfer in one hand and increase the entropy generation by their excessive pressure drop in other hand. The Optimum design of a thermal system is achieved when the entropy generation is minimized (see Bejan [21]). In other words, the best design is the case with maximum possible heat transfer performance and minimum pressure drop.

It can be realized from above review that most of previous studies are focused separately on the effect of nanofluids flow in smooth tubes for heat transfer enhancement and pressure drop augmentation and, limited data have been reported about turbulent nanofluid flows in tubes with ribs or grooves. The lack of study of entropy generation minimization in turbulent flow of nanofluids inside

grooved tubes is the motivation for this paper. For example, the optimum geometric ratios of grooves have not been presented for this case. In this paper, the convective heat transfer of Al_2O_3-water nanofluid in a tube with rectangular grooves is numerically studied. The entropy generation is used as a criterion to find the optimum geometric ratio of the rectangular groove. Some correlations for Nusselt number in grooved tubes are presented. The variations of Nusselt number, friction factor and the entropy generation number for different conditions are also investigated in detail.

2. Mathematical formulation

2.1 Problem description

The geometry of the problem is shown in Fig. 1. It consists of a tube with a smooth section of a length 66D in its entrance to ensure a developed flow. A grooved section of a length 33D is attached to the smooth tube. The Tube diameter is 36 mm. The ratio of tip width (t) to base width (p) ratio is the main variable in this study. It is in the range of 0.2-2. The grooves have constant height of e=3 mm and base width of p=6 mm. For example, at groove ratio of t/p=1, the length of grooves tip is t=6 mm. Details of the grooves are shown in Fig1.b. The Constant heat transfer rate of 10000 Watts is considered on grooved section of the tube. Nanofluid enters the domain at the inlet with the uniform velocity and temperature.

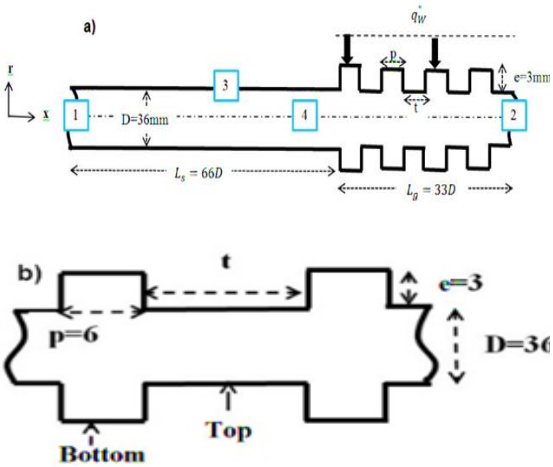

Fig.1 Geometry details for
(a) whole domain, (b) details of rectangular grooves (all dimension are in mm).

2.2 Thermophysical properties of nanofluids

The thermophysical properties of Al_2O_3-water nanofluid with a nanoparticle mean diameter of 20 nm are obtained using the assumption of single-phase model. The Calculation of the nanofluid density is based on the classical theory of mixtures, which is proposed by Maxwell [22] as

$$\rho_{nf} = (1-\varphi)\rho_{bf} + \varphi\rho_p \tag{1}$$

Where, ρ_{bf} and ρ_p are the densities of the base fluid and the nanoparticles, respectively.

Xuan and Roetzel [23] proposed to calculate specific heat capacity of the nanofluid using the following equation:

$$c_{p_{nf}} = \frac{(1-\varphi)(\rho c_p)_{bf} + \varphi(\rho c_p)_p}{\rho_{nf}} \tag{2}$$

Where, c_{pbf} and c_{pp} are the specific heat capacity of the base fluid and nanoparticle, respectively.

Corcione [24] propose to calculate the nanofluids viscosity by

$$\frac{\mu_{nf}}{\mu_{bf}} = \frac{1}{1-34.87\left(\frac{d_p}{d_{bf}}\right)^{-0.3}\varphi^{1.03}} \tag{3}$$

In the above equation d_{bf} is the equivalent molecular diameter of the base fluid which is given by

$$d_{bf} = 0.1\left[\frac{6M}{N\pi\rho_{f0}}\right]^{\frac{1}{3}} \tag{4}$$

Where M is the molecular weight of the base fluid, N is the Avogadro number $\left(6.022\times10^{23}, mol^{-1}\right)$ and ρ_{f0} is the density of base fluid at $T_0 = 293K$.

In order to evaluate the thermal conductivity of the nanofluid $\left(k_{nf}\right)$, Chon *et al.* [25] proposed the following equation:

$$\frac{k_{nf}}{k_{bf}} = 1+64.7\varphi^{0.746}\left(\frac{d_{bf}}{d_p}\right)^{0.369}\left(\frac{k_p}{k_{bf}}\right)^{0.7476} \mathrm{Pr}^{0.9955}\,\mathrm{Re}^{1.2321} \tag{5}$$

The Prandtl number (Pr), and the Reynolds number (Re) in above equation are defined by Chon *et al.* [25]. The thermo-physical properties of

the water and Al_2O_3 nanoparticles selected from Refs. [26, 27] are shown in table 1.

2.3 Governing equation

Reynolds averaged Navier Stokes and continuity equations are solved in the axisymmetric form for a turbulent, two-dimensional, steady-state, and incompressible flow (See e.g. White [28] and Versteeg and Malalasekera [29]).

Continuity equation:

$$\frac{1}{r}\frac{\partial(rV_r)}{\partial r}+\frac{\partial V_x}{\partial x}=0 \tag{6}$$

Momentum equations:

$$V_r\frac{\partial V_x}{\partial r}+V_x\frac{\partial V_x}{\partial x}=-\frac{1}{\rho}\frac{\partial p}{\partial x}+\frac{1}{\rho}\left[\frac{1}{r}\frac{\partial}{\partial r}\left(r(\mu+\mu_t)\frac{\partial V_x}{\partial r}\right)+\frac{\partial}{\partial x}\left((\mu+\mu_t)\frac{\partial V_x}{\partial x}\right)\right] \tag{7}$$

$$V_r\frac{\partial V_r}{\partial r}+V_x\frac{\partial V_r}{\partial x}=-\frac{1}{\rho}\frac{\partial p}{\partial r}+\frac{1}{\rho}\left[\frac{1}{r}\frac{\partial}{\partial r}\left(r(\mu+\mu_t)\frac{\partial V_r}{\partial r}\right)+\frac{\partial}{\partial x}\left((\mu+\mu_t)\frac{\partial V_r}{\partial x}\right)-\frac{V_r}{r^2}(\mu+\mu_t)\right] \tag{8}$$

Energy equation:

$$V_x\frac{\partial T}{\partial x}+V_r\frac{\partial T}{\partial r}=\frac{1}{\rho c_p}\left[\frac{1}{r}\frac{\partial}{\partial r}\left(r(k+k_t)\frac{\partial T}{\partial r}\right)+\frac{\partial}{\partial x}\left((k+k_t)\frac{\partial T}{\partial x}\right)\right] \tag{9}$$

Where μ_t and k_t are the turbulent viscosity and conductivity and given as:

$$k_t=\frac{c_p\mu_t}{\sigma_t} \tag{10}$$

$$\mu_t=C_\mu\rho\frac{k^2}{\varepsilon} \tag{11}$$

μ_t needs to be modeled by k-ε model. Versteeg and Malalasekera [29] expressed k-ε turbulence model equations for turbulent kinetic energy (k) as

$$\frac{1}{r}V_r\frac{\partial(rk)}{\partial r}+V_x\frac{\partial(k)}{\partial x}=\frac{1}{\rho}\left[\frac{1}{r}\frac{\partial}{\partial r}\left(r\left(\mu+\frac{\mu_t}{\sigma_k}\right)\frac{\partial k}{\partial r}\right)+\frac{\partial}{\partial x}\left(\left(\mu+\frac{\mu_t}{\sigma_k}\right)\frac{\partial k}{\partial x}\right)\right]+G_k-\rho\varepsilon \tag{12}$$

And for turbulent dissipation rate (ε) the transport equation is given by

$$\frac{1}{r}V_r\frac{\partial(r\varepsilon)}{\partial r}+V_x\frac{\partial(\varepsilon)}{\partial x}=\frac{1}{\rho}\left[\frac{1}{r}\frac{\partial}{\partial r}\left(r\left(\mu+\frac{\mu_t}{\sigma_\varepsilon}\right)\frac{\partial\varepsilon}{\partial r}\right)+\frac{\partial}{\partial x}\left(\left(\mu+\frac{\mu_t}{\sigma_\varepsilon}\right)\frac{\partial\varepsilon}{\partial x}\right)\right]+C_{1\varepsilon}\frac{\varepsilon}{k}G_k-C_{2\varepsilon}\rho\frac{\varepsilon^2}{k} \tag{13}$$

Where G_k is the rate of production of turbulent kinetic and $\rho\varepsilon$ is its destruction rate. G_k is given by:

$$G_k=\mu_t\left|\nabla V+\nabla V^T\right|^2 \tag{14}$$

σ_k and σ_ε are turbulent Prandtl numbers for the turbulent kinetic energy and dissipation rate respectively. C_μ, $C_{1\varepsilon}$ and $C_{2\varepsilon}$ are the model constants. These constants are given in Table 2.

At the inlet, the values of k and ε are calculated using turbulence intensity (I) which is calculated by

$$I=0.16\,\mathrm{Re}^{-1/8} \tag{15}$$

Entropy generation is calculated using second law of thermodynamic for the control volume. The Balance of entropy generation is given by the following equation.

$$\dot{S}_{gen}=\int_{outlet}S_{out}d\dot{m}_{out}-\int_{inlet}S_{in}d\dot{m}_{in}-\int\frac{q''}{T}dA \tag{16}$$

Reynolds number (Re), average Nusselt number ($\overline{Nu}$), flow friction factor (f) and entropy generation ratio ($N_{s,a}$) are given by

$$\mathrm{Re}=\frac{\rho_{nf}V_{avg}D}{\mu_{nf}} \tag{17}$$

$$\overline{Nu}=\frac{\bar{h}\cdot D}{k_{nf}}=\frac{q''}{\left(\overline{T_w}-\overline{T_b}\right)}\cdot\frac{D}{k_{nf}} \tag{18}$$

Where, q" is heat flux. $\overline{T_w}$ and $\overline{T_b}$ represent the average wall temperature and bulk fluid flow temperature, respectively (See Bilen *et al.*[7]).

$$f=\frac{2(\Delta p)}{\left(\frac{L}{D}\right)\cdot\rho_{nf}\cdot V_{avg}^2} \tag{19}$$

Where L is the developed flow length.

Table 1.Thermo-physical properties of materials.

	ρ(kg/m^3)	c_p(J/kg.K)	k(W/m.K)	μ(kg/m.s)
Water (See White [26])	997.47	4180	0.6	9.45×10^{-4}
Al_2O_3[27]	3890	880	36	-

Table 2. Constants in the k-ε turbulence model transport equations [29].

σ_t	σ_k	σ_ε	$C_{1\varepsilon}$	$C_{2\varepsilon}$	C_μ
0.85	1	1.3	1.44	1.92	0.09

$$N_{s,a} = \dot{S}'_{gen,a} / \dot{S}'_{gen,0} \quad (20)$$

Where $\dot{S}'_{gen,a}$ represents entropy generation rate per length in the test section (grooved section of the tube) and $\dot{S}'_{gen,0}$ represents entropy generation rate per length in the reference section (base fluid flow inside a smooth tube with the same length). The system will be thermodynamically advantageous if $N_{s,a}$ values are less than 1.

The Governing equations are solved by the following boundary conditions: (1) Uniform velocity and temperature of 22 C at the inlet, (2) Zero gradient for velocity at the outlet, (3) No slip conditions for velocity and enhanced wall treatment (a combination of two layer model and enhanced wall functions) for the turbulence parameters, and (4) axisymmetric condition for the axis.

2.4 The Numerical procedure

In this study, the governing equations (Eqs. (7) to (13)), were discretized using the finite volume method. The SIMPLE algorithm is used for pressure velocity coupling. The second order upwind scheme is applied to discrete the momentum, turbulent kinetic energy, turbulent dissipation rate, and energy equations (See Vesteeg and Malalasekera [29]). The iterative procedure is terminated when the residuals are lower than 10^{-5}. The whole solution domain is considered as a control volume and Eq. 16 was applied to calculate the total entropy generation at the same control volume. The Different integrals of this equation were evaluated by using the obtained numerical result from the solution of the governing equations.

In order to check out the grid independency of the solution, several structured and unstructured meshes were generated. As an example, the structured mesh for grooved tube is shown in Fig. 2. Changes in predicted average Nusselt number for different meshes are compared in table 3.

As can be seen, the appropriate number of cells for suitable accuracy and solution time in smooth and grooved tubes (with ratio t/p=1) are 400,000 1,400,000 respectively. In order to select the appropriate turbulence model, the variations of average Nusselt number with the flow Reynolds number for smooth and grooved tubes are compared in Fig. 3. The results for smooth tube are compared with correlations of Pak and Cho [12], Xuan and Li [13] and Maiga*et al.* [14] for Al_2O_3-water nanofluid.

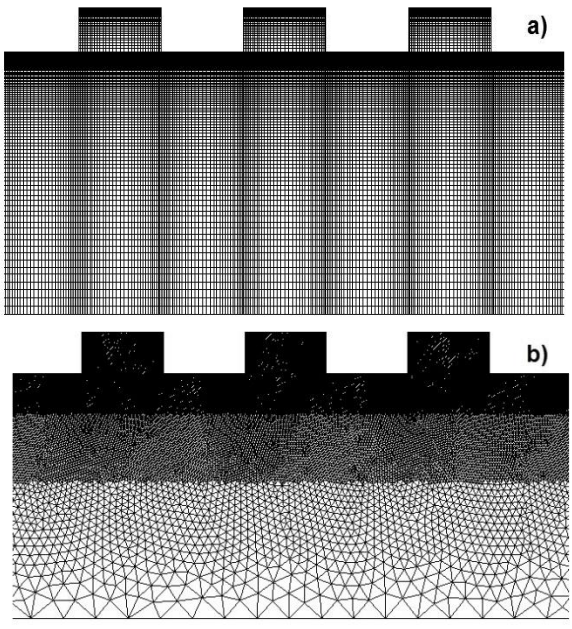

Fig. 2 Meshes for grooved tube a) structured b) unstructured mesh.

Table 3. Grid independency test results.

Geometry	Mesh Type	Number of cells	Changes in Average Nu (%)
Smooth tube	Structured	400000	0.02
		600000	
Rectangular grooved tube	Structured	1400000	0.15
		1600000	0.07
		1800000	

Fig 3 (a) indicates a good agreement between the results of present work and those obtained by the previous correlations for the Al_2O_3-water nanofluid flow in the smooth tube. The differences between the obtained results and correlations of Xuan and Li [13], Pak and Cho [12] and Maiga *et al.*[14] are 4, 5, and 18%, respectively which shows the applicability of the applied model.

For validation of the numerical simulations in the grooved tube, the simulations results for airflow with t/p=1 are compared with experimental data of Billen *et al.* [6] in Fig 3(b). It can be concluded that the standard k-ε, RNG k-ε with enhancement wall treatment, and Reynolds Stress Transport Model (RSTM) yield the better predictions with the maximum deviations of 6, 8 and 9%, respectively. The Standard k-ε model with enhancement wall treatment has been chosen for the simulations.

3. Result and discussion

Fig. 4 displays the effects of Al_2O_3 nanoparticles volume fraction on the average Nusselt number in a grooved tube with geometric ratio of t/p=1. The results indicate that by increasing the nanoparticles volume fraction and flow Reynolds number, the average Nusselt number will enhance. For the volume fraction of 3% and at the Reynolds number of 30,000, the average Nusselt number is increased by 6%.

Adding nanoparticles have an adverse effect on the viscosity of the nanofluid and causes more pressure drops. Fig. 5 indicates the ratio of the pressure drop for the nanofluid flow to that of the base fluid flow at different Reynolds numbers and different nanoparticles volume fractions. Adding 3% of nanoparticles to water will approximately double the pressure drop.

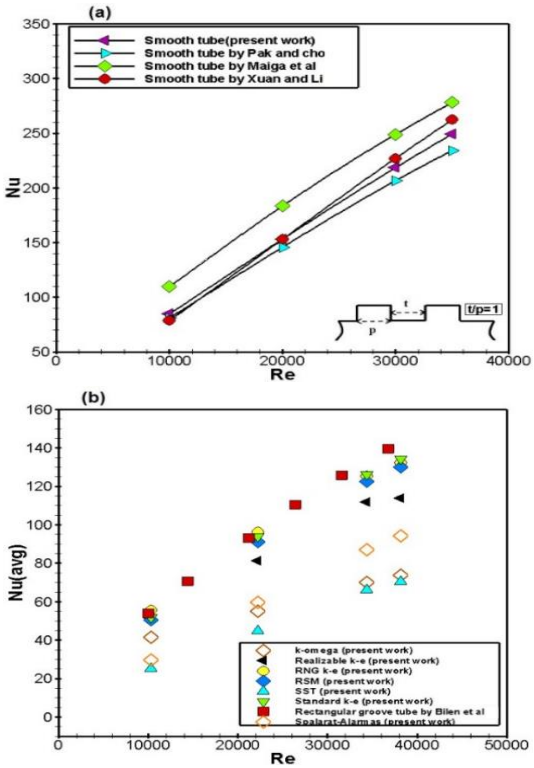

Fig. 3 Comparison between the predicted average Nusselt number and a) available correlations for Al_2O_3-water nanofluid in a smooth tube, b) experimental data of Bilen *et al.* [7] for airflow inside a grooved tube (t/p=1).

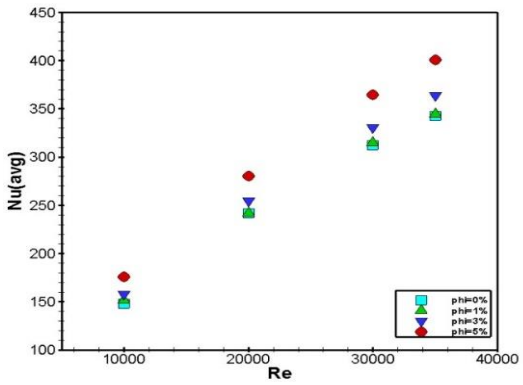

Fig. 4 The influences of the Al_2O_3 nanoparticles volume fraction on the average Nusselt number for different Reynolds numbers of the flow in a grooved tube (t/p=1).

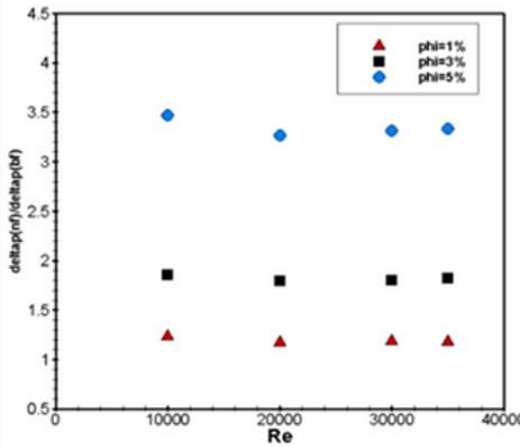

Fig. 5 Variations of the flow pressure drop ratio with nanoparticles volume fraction on in grooved tube (t/p=1).

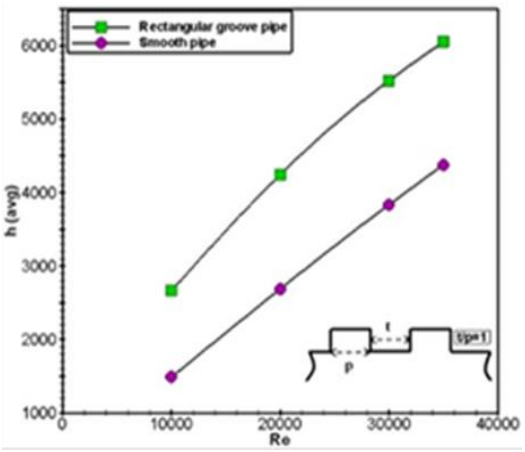

Fig. 6 Variations of average convection heat transfer coefficient with flow Reynolds number for grooved and smooth tubes ($\varphi = 0.01$ and t/p=1)

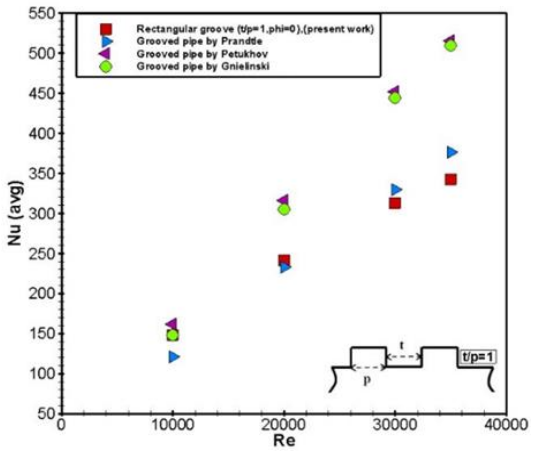

Fig. 7 Comparison between the result of the present work and available correlations for average Nusselt number of the water flow in a grooved tube with t/p=1.

Fig. 6 displays the influences of the rectangular grooves on the average heat transfer coefficient. The results are presented for nanoparticles volume fraction of φ=0.01. Fig. 7 shows that for flow Reynolds number of Re=20,000, by using grooved tube with geometric ratio of t/p=1, the average convection heat transfer coefficient enhancement of 58% will be obtained. This is due to greater production of turbulence, increase in the heat transfer area, and more flow mixing inside the grooved tube. The existence of the grooves provides the periodic redevelopment of the boundary layers over their tip that causes a more effective heat transfer.

Nusselt number for the flows with Reynolds numbers in the range of 10,000–35,000 inside the grooved tube (t/p=1) are compared with the results of correlation obtained by Prandtl (see Eckert [30]), Petukhove [31], and Gnielinski [32] in Fig. 7. The mentioned correlations are as follows:

Prandtl's correlation:

$$\frac{Nu}{\mathrm{Re}\,\mathrm{Pr}} = \frac{f/8}{1+8.7(f/8)^{1/2}(\mathrm{Pr}-1)} \tag{21}$$

Petukhove's correlation:

$$\frac{Nu}{\mathrm{Re}\,\mathrm{Pr}} = \frac{f/8}{1.07+12.7(f/8)^{1/2}(\mathrm{Pr}^{2/3}-1)} \tag{22}$$

And Gnielinski's correlation:

$$Nu = \frac{(f/8)(\mathrm{Re}-1000)\,\mathrm{Pr}}{1+12.7(f/8)^{1/2}(\mathrm{Pr}^{2/3}-1)} \tag{23}$$

This figure shows that the results obtained from present work for grooved tube are in the same order of the results obtained by previous correlations. However, in low Re numbers the Prandtl's formula deviates from the results of the present work and in

the flows with high Re number, the results of Gnielinski and Petukhove formulas are greater than that of the present work. It should be noted that the above correlations were designed for sand grain pipe roughness and absolutely their predictions have some deviations for grooved pipes.

The Variations of the local convection heat transfer coefficient at the grooved tube wall is compared with that of the smooth tube for Re=20,000 and φ=0.03 in Fig. 8. As can be seen, obtained h(x) for smooth tube has a decreasing trend. For a grooved tube, the variations of the heat transfer coefficient are quite complex. At the base of the groove a dead zone forms and the heat transfer coefficient is low due to lower velocity of the flow. However by proceeding in axial direction, the flow velocity in the near wall region increases which leads to higher heat transfer coefficients. When the flow reaches the tip of the groove, maximum local heat transfer coefficient occurs. Here, the variations of the heat transfer coefficient are similar to that of a boundary layer flow over a flat plate. These variations are repeated periodically but with reduced amplitude.

The friction factor of the grooved tube is higher than that of the smooth tube. At the Reynolds number of 20,000, the friction factors of the grooved tube are 4 and 3 times the friction factor of smooth tube for the geometric ratios of t/p=0.5 and t/p=1, respectively.

Using the obtained numerical results, three different correlations are proposed here for the calculation of the average Nusselt numbers.

For smooth tubes:

$$\overline{Nu} = 0.02\,\mathrm{Re}^{0.8264}\,\mathrm{Pr}^{0.4019} \tag{24}$$

For grooved tubes with t/p=1

$$\overline{Nu} = 0.2076\,\mathrm{Re}^{0.6421}\,\mathrm{Pr}^{0.3763} \tag{25}$$

And for grooved tubes with t/p=0.5

$$\overline{Nu} = 0.3255\,\mathrm{Re}^{0.5806}\,\mathrm{Pr}^{0.5244} \tag{26}$$

The maximum deviations of the predicted average Nusselt numbers from the above correlations are 0.48% for smooth tube and 0.72% and 0.56%, for grooved tube with t/p=1 and t/p=0.5, respectively.

Fig. 10 shows the effects of the groove geometric ratio (t/p) on the average Nusselt number for grooved tubes at the Reynolds number of 10,000. The results show that the lower values of t/p can increase the average Nusselt number. The highest values of average Nusselt number occurs at t/p=0.2. For lower geometric ratios, the higher Nusselt numbers are obtained. However as mentioned in the following sections, from the second law of thermodynamic, the entropy generation ratio is minimum at the geometric ratio of 0.25.

The flow patterns near the grooves for different values of t/p are shown in Fig. 11. For smaller values of the t/p, there is more flow mixing due to shorter distance for circulation. This flow mixing increases the heat transfer coefficients and friction factors.

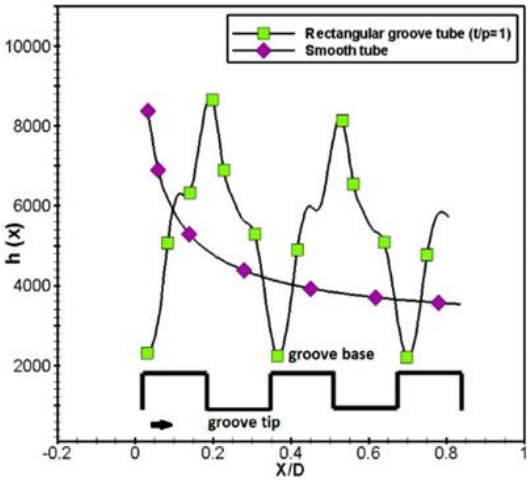

Fig. 8 Comparison between local heat transfer coefficient at the rectangular grooves (t/p=1, φ=0.01, and Re=20000) and smooth tube wall.

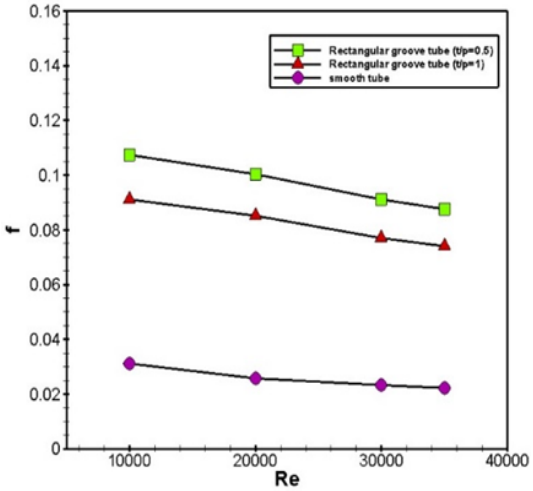

Fig. 9 The predicted friction factors for grooved and smooth tubes versus the flow Reynolds numbers.

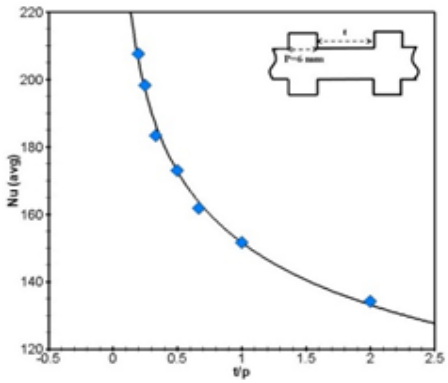

Fig. 10 Variations of the average Nusselt number as a function of the geometric ratio (t/p) at Re=10,000 and φ=0.01.

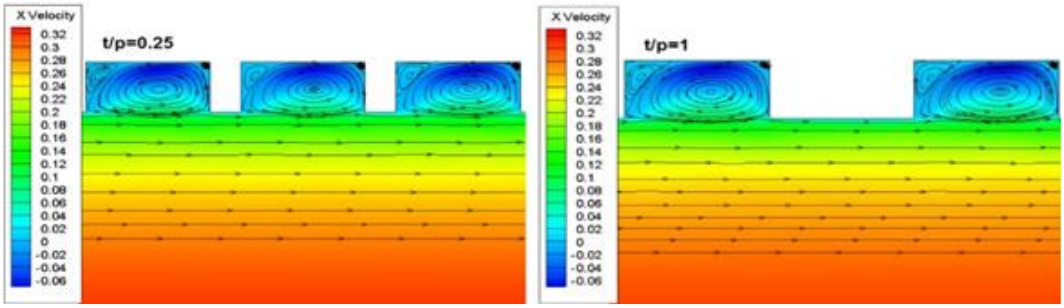

Fig. 11 Flow patterns near the grooves for different values of t/p (φ=0.01, Re=10000) (velocities are in m/s).

The Variations of the friction factor with the geometric ratios of t/p are shown in Fig. 12. The highest values of the friction factor is obtained at geometric ratio of t/p=0.2. From the previous discussion, it is evident that adding nanoparticles and grooves can enhance the convection heat transfer coefficients but both of them increase the pressure drop. The total entropy generation rate can be used as a criterion for evaluation the effects of the parameters. For this purpose, the Entropy generation ratio ($N_{s,a}$) is used (See Eq. (20)).

Variations of Entropy generation ratio by nanoparticles volume fraction at different flow Reynolds number for t/p=1.0 is shown in Fig. 13.

Fig.13 Variations of Entropy generation ratio by nanoparticles volume fraction at different flow Reynolds number (t/p=1.0)

As shown, the entropy generation ratio has a decreasing trend which shows the good performance of the heat transfer enhancement methods by adding the nanoparticles and grooves to the tube.

Fig. 14 shows the effects of groove geometric ratio (t/p) on entropy generation ratio for grooved tube. The flow Reynolds number is 10,000 and nanoparticles volume fraction of φ=0.01 is considered for these simulations. It is seen from the figure that for all ratios of t/p the use of grooved tube is thermodynamically advantageous ($N_{s,a}$<1). This is because of reduction in irreversibility of the heat transfer process overcomes the negative effects of the pressure drop. These results also show that the minimum entropy generation ratio occurs at the ratio of t/p=0.25. This is the optimum ratio for the rectangular grooved tube.

In order To study the effects of adding the nanoparticles, Fig. 15 indicates the entropy generation ratio of water-Al_2O_3 flow versus volume fraction of nanoparticles in the optimum ratio of grooved tube (t/p=0.25) for flow with the Reynolds number of 10,000.

It is shown that the entropy generation ratio decreases by adding the nanoparticles almost linearly. This figure shows that the entropy generation ratio will decrease about 25% by adding 5% of nanoparticle volume fraction

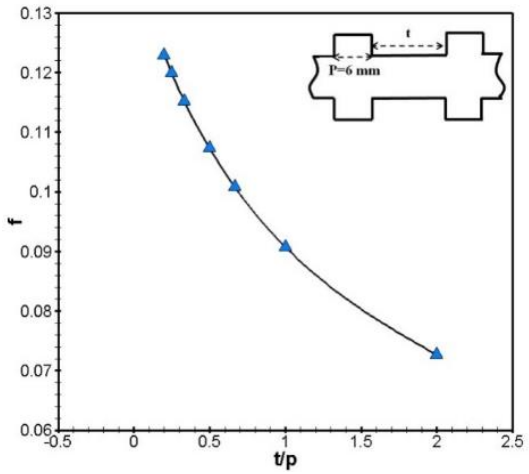

Fig. 12 The effects of the geometric ratio (t/p) on the friction factor (Re=10,000).

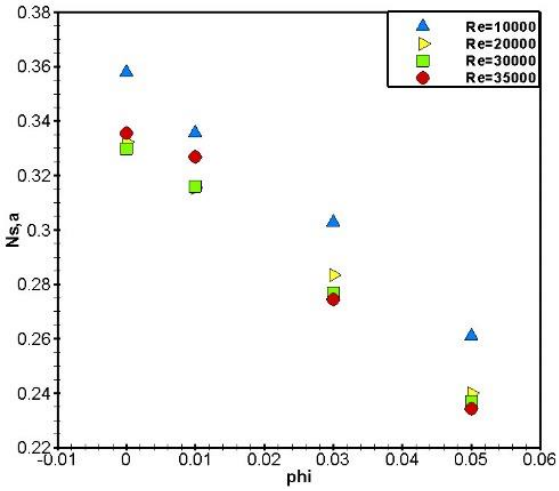

Fig.13 Variations of Entropy generation ratio by nanoparticles volume fraction at different flow Reynolds number (t/p=1.0)

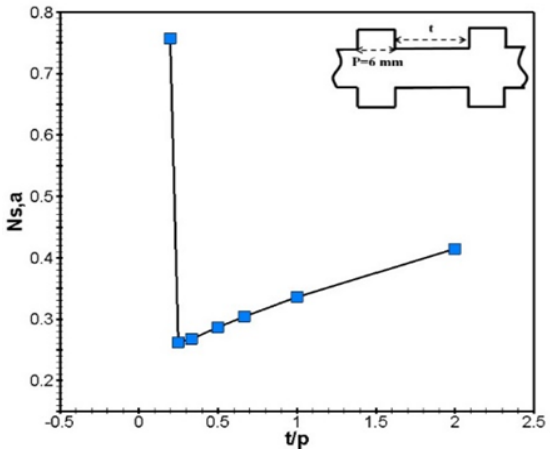

Fig. 14 Variations of the Entropy generation ratio with groove ratio (t/p) (Re=10000, φ=0.01).

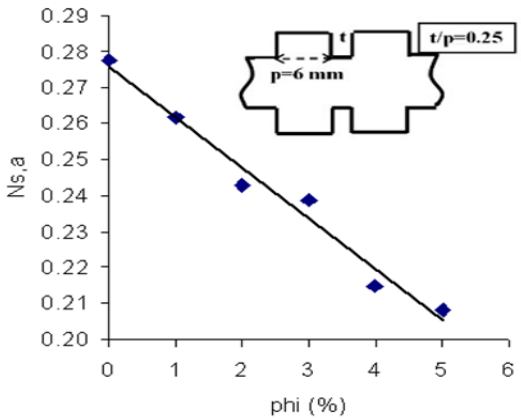

Fig. 15 The effect of nanoparticles volume fraction (φ) on the entropy generation ratio (Re=10,000 and t/p=0.25).

4. Conclusions

The comparison between the predicted results obtained by the different turbulence models and available experimental data shows that the standard k-ε and RNG k-ε models with enhancement wall treatment give the better predictions than other examined turbulence models. The main parameter of this study is the ratio of grooves tip width to their base width (t/p). The average enhancement in heat transfer coefficient for grooved tube with t/p=1 is 58% at Re=20,000.

The flow friction factor in the grooved tube with geometric ratio of t/p=0.5 and t/p=1 are about 4 and 3 times of that of the smooth tube at Reynolds number of 20,000. It was shown that for smaller values of the t/p, the flow mixing occurs the more times. This flow mixing increases the heat transfer coefficient and flow friction factor. The highest values of average Nusselt number is obtained at t/p=0.2 for the grooved tubes. By applying the nanofluid, a significant increase in the pressure drop is observed, especially in the higher Reynolds number. This is the disadvantage of use of the nanofluids.

It was shown that the turbulent heat transfer of nanofluid flow in grooved tubes is thermodynamically advantageous. The results indicate that the entropy generation ratio for the grooved tube with geometric ratio of t/p=0.25 is minimized. This ratio can be selected as the optimum value of the geometric ratio.

Nomenclature

t	ribs tip width, mm	ρ	density, kg/m^3
p	ribs tip width, mm	c_p	specific heat capacity, J/kg.K
k	turbulence kinetic energy, m^2/s^2	μ	viscosity, N.s/m^2
ε	turbulence dissipation rate, m^2/s^3	M	molecular weight, g/mol
θ	degree, °c	N	Avogadro constant (= $6.022\times10^{23}\left(mol^{-1}\right)$)
D	diameter, mm	T	temperature, K
e	equivalent roughness height, mm	k	thermal conductivity, W/m.K
Nu	Nusselt number (=hD/k)	α	thermal distribution, m^2/s
φ	Nanoparticles volume fraction	V	velocity, m/s
Re	Reynolds number (= $\frac{\rho VD}{\mu}$)	κ_B	Stefan-Boltzmann constant (= $1.3807\times10^{-23}\left(J/K\right)$)
Pr	Prandtl number (= $\frac{\upsilon}{\alpha}$)	l_{bf}	mean free path, nm
Pe	Peclet number (= $\frac{u.d}{\alpha}$)	P	pressure, Pa
n	number of the ribs	σ_t	turbulent Prandtl number
σ_k	turbulent Prandtl number for k	Subscripts	
σ_ε	turbulent Prandtl number for ε	nf	Nanofluid
I	turbulent intensity	s	Smooth
$\dot{m}$	mass flow rate, kg/s	g	Grooved
A	area, m^2	bf	Base fluid
$\dot{S}'$	rate of entropy per unit length (W/mK)	p	Particle
f	friction factor	Br	Brownian
$N_{s,a}$	Entropy generation ratio (= $\frac{\dot{S}'_{gen,a}}{\dot{S}'_{gen,0}}$)	t	Turbulence
L	Length, m	gen	Generation
h	convective heat transfer coefficient, W/m^2 K	a	Augmented
Q	heat transfer rate, W	0	Reference conditions
		w	Wall

References

[1]. Cheng, L. "Nanofluid heat transfer technologies," Recent Pat. Eng. 3 (2009) 1-7.

[2]. Duangthongsuk, W., Wongwises, S. "An experimental study on the heat transfer performance and pressure drop of TiO2–water nanofluids flowing under a turbulent flow regime," International Journal of Heat and Mass Transfer, 53 (2010) 334–344.

[3]. Webb, R.L., Robertson, G.F., "Shell-side evaporators and condensers used in the refrigeration industry," in: R.K. Shah, E.C. Subbarao, R.A. Mashelkar (Eds.), Heat Equipment Design, (Hemisphere Pub. Corp., Washington), pp. 559-570 (1988).

[4]. Dalle Donne, M., Meyer, L. "Turbulent convective heat transfer from rough surfaces with two-dimensional rectangular ribs," International Journal Heat and Mass Transfer 20 (1977) 583–620.

[5]. Naphon, P., Nuchjapo, M., Kurujareon, J., "Tube side heat transfer coefficient and friction factor characteristics of horizontal tubes with helical rib," Energy Conversion and Management 47 (2006) 3031–3044.

[6]. San, J.Y., Huang, W.C. "Heat transfer enhancement of transverse ribs in circular tubes with consideration of entrance effect," International Journal of Heat and Mass Transfer 49 (17, 18) (2006) 2965–2971.

[7]. Bilen, K., Cetin, M., Gul, H., Balta, T. "The investigation of groove geometry effect on heat transfer for internally

grooved tubes," Applied Thermal Engineering 29 (2009) 753–761.
[8]. Pingan, L., Ye, G., Hairong, M., Liu, H. "Numerical simulation of heat transfer and resistance pattern in channels with different ribs," in: 2010 International Conference on Computer Design and Applications (ICCDA 2010) p. V3-507-V3-11.
[9]. Choi, S.U.S. "Enhancing thermal conductivity of fluids with nanoparticles," ASME Publications FED-Vol. 231/MD-Vol. 66, (1995)99- 105,
[10]. Keblinski, P., Phillpot, S.R., Choi, S.U.S., Eastman, J.A. "Mechanisms of heat flow in suspensions of nano-sized particles (nanofluid)." International Journal of Heat and Mass Transfer, 45 (2002) 855-863.
[11]. Das, S., Putra, N., Thiesen, P., Roetzel, W. Temperature dependence of thermal conductivity enhancement for nanofluids, Journal of Heat Transfer 125 (2003) 567–574.
[12]. Pak, B.C., Cho, Y.I. Hydrodynamic and heat transfer study of dispersed fluids with submicron metallic oxide particles, Experimental Heat Transfer 11 (1998) 151–170.
[13]. Xuan, Y.M., Li, Q. Investigation on convective heat transfer and flow features of nanofluids, Journal of Heat Transfer 125 (2003) 151–155.
[14]. Maiga, S.E.B., Nguyen, C.T., Galanis, N., Roy, G., Mare, T., Coqueux, M. "Heat transfer enhancement in turbulent tube flow using Al2O3 nanoparticle suspension," International Journal of Numerical Methods for Heat and Fluid Flow 16 (2006) 275–292.
[15]. Fotukian, S.M.,Nasr Esfahany, M. Experimental investigation of turbulent convective heat transfer of dilute γ-Al2O3/water nanofluid inside a circular tube, International Journal of Heat and Fluid Flow, 31 (2010) 606–612.
[16]. Wongcharee, K., Eiamsa-ard, S. Heat transfer enhancement by using CuO/water nanofluid in corrugated tube equipped with twisted tape, International Communication of Heat and Mass Transfer 39 (2) (2012) 251–257.
[17]. Manca, O., Nardini, S., Ricci, D. A numerical study of nanofluid forced convection in ribbed channels, Applied Thermal Engineering 37 (2012) 280–292.
[18]. Vatani, A., Mohammed, H.A. Turbulent nanofluid flow over periodic rib-grooved channels, Engineering Applications of Computational Fluid Mechanics 7(3) (2013) 369-381.
[19]. Haghighi, E.B., Utomo, A.T., Ghanbarpour, M., Zavareh, A.I.T., Poth, H., khodabandeh, R., Pacek, A., Palm, B.E. Experimental study on convective heat transfer of nanofluids in turbulent flow: Methods of comparison and their performance, Experimental thermal and Fluid Sciences, 57 (2014) 378-387.
[20]. Al-Shamani, A.N., Sopian, K., Mohammed, H.A., Mat, S., Ruslan, M.H., Abed, A.M. "Enhancement heat transfer characteristics in the channel with trapezoidal rib-groove using nanofluids, Case Studies in Thermal Engineering, 5, (2015) 48-58.
[21]. Bejan, A. Entropy Generation Minimization, CI Boca Taron (1996).
[22]. Maxwell, J.C. A treatise on Electricity and Magnetism, Carendon Press, Oxford UK (1873).
[23]. Xuan, Y.M., Roetzel, W. "Conceptions for heat transfer correlation of nanofluids," International Journal of Heat and Mass Transfer 43 (2000) 3701–3707.
[24]. Corcione, M. "Empirical correlating equations for predicting the effective thermal conductivity and dynamic viscosity of nanofluids," Energy Conversion Management. 52 (2011) 789-793.
[25]. Chon, C.H., Kihm, K.D., Lee, S.P., Choi, S.U.S. "Empirical Correlation Finding the Role of Temperature and Particle Size for Nanofluid (Al2O3) 70 Conductivity Enhancement," Appl. Phys. Lett., 153107.
[26]. White, F.M. "Fluid Mechanics", 7th ed. McGraw-Hill, New York (2011).
[27]. www.US-Nano.com.
[28]. White, F.M. "Viscous fluid Flow," 3rd ed., McGraw-Hill, New York (2003).
[29]. Versteeg, H., Malalasekera, W. An introduction to computational fluid dynamics: the finite volume method, 2nd ed. Pearson Education Limited (2007).
[30]. Eckert, E.R.G., Drake, R.M. Heat and Mass Transfer, McGraw-Hill, New York (1959).
[31]. Petukhov, B.S. "Heat transfer and friction in turbulent pipe flow with variable physical properties," Adv. Heat Transfer 6 (1970) 503–564.
[32]. Gnielinski, V. "New Equations for Heat and Mass Transfer in Turbulent Pipe and Channel Flow," International Chemical Engineering 16 (1976) 359–368.